Time-Resolved Spectroscopy of ZnTe Photocathodes for Solar Fuel Production

Xianqiang Xiong,[a,b] *Mark Forster,*[a] *Jonathan D Major,*[a] *Yiming Xu*[b] *and Alexander J. Cowan**[a]

[a]University of Liverpool, Stephenson Institute for Renewable Energy, Department of Chemistry, Liverpool, L69 7ZF, United Kingdom. E-mail:acowan@liverpool.ac.uk

[b]Zhejiang University, State Key Laboratory of Silicon Materials and Department of Chemistry, Hangzhou, 310027, China. E-mail: xuym@zju.edu.cn.

Abstract. The negative conduction band potential and small bandgap of ZnTe makes the material a promising photoelectrode for solar fuels production, photocatalyst and solar cell component. However, the factors controlling the underlying efficiencies of the light driven processes on ZnTe are not well understood. Here we report a combined spectroelectrochemical and transient absorption (TA) spectroscopic investigation of ZnTe photoelectrodes for CO_2 reduction. In the visible region TA spectra are dominated by a broad positive photoinduced absorption at 540 nm following initial charge carrier relaxation (< 540 nm). The 540 nm spectral feature is shown to be related to deeply trapped photoelectrons with charge carrier recombination occurring via a trapping-detrapping model on the microsecond timescale. Significantly these deeply trapped electrons are insensitive to the presence of electron acceptors and to the applied potential of the ZnTe electrode. Trapping at such states is proposed to be a significant factor limiting the photoelectrochemical activity of ZnTe. nIR spectral features associated with shallow trapped electrons exist at > 1150 nm. Shallow trapped electrons are generated

and accumulate at potentials where photoelectrochemical H_2 evolution and CO_2 reduction occurs and we show these charges are able to undergo interfacial electron transfer to an acceptor molecule. The passivation of sites related to deep traps is proposed to be the key to optimize the photocatalytic and photoelectrochemical performance of ZnTe.

1. INTRODUCTION

Sunlight is the most abundant natural resources available on earth and has the potential to meet mankind's future energy needs. Photoelectrochemical (PEC) water splitting and CO_2 reduction for solar energy production offers a completely sustainable route to produce energy with only sunlight, water and CO_2 as the inputs.[1-2] Although significant progress has been made in developing photocatalytic and photoelectrocatalytic materials for water oxidation and CO_2 reduction in recent years, the efficiency of scalable materials remains insufficient for practical application. It is widely accepted that a significant limiting factor for many photoelectrodes is a mismatch between the timescales of charge recombination and interfacial charge transfer reactions.[3] As such, it is imperative to understand the underlying photophysical processes that affect the photoactivity of semiconductor materials.

Recently, ZnTe has attracted considerable attention as a promising p-type semiconductor due to its successful application for both H_2 evolution and CO_2 reduction under visible light irradiation.[4-12] Although the photocatalytic and photoelectrocatalytic performance for water splitting and CO_2 reduction obtained with this material are still relatively low, ZnTe attracts considerable attention due to desirable properties including a small direct band gap of ~ 2.26 eV allowing for efficient visible light absorption in the solar spectrum[13] and a very negative conduction band edge position (-1.63 V *vs* RHE)[14] which provides a large thermodynamic driving force for photoelectron transfer for both proton reduction and

CO_2 reduction. To date most of the studies regarding ZnTe are mainly focused upon the synthesis and/or photo(electro)catalytic performance. Of particular note are studies where ZnTe/ZnO heterojunctions have been utilized to significantly improve photocurrent densities during CO_2 reduction,[4-7, 10-12] carbon and MoS_2 modification of ZnTe materials with enhanced activity for H_2 production,[7] polypyrrole-coated ZnTe to address the selectivity towards CO_2,[8] and oxygen incorporation for enhanced stability.[9] In contrast there are few studies regarding the charge carrier dynamics of ZnTe and the potential loss mechanisms occurring following photon absorption. It is therefore important that attempts are made to understand the origin of photocatalytic and photoelectrocatalytic activity for ZnTe so that new strategies to prepare efficient ZnTe-based materials can be developed.

Transient absorption (TA) spectroscopy is a useful tool to monitor charge carrier trapping, recombination and transfer process for semiconductor materials and has successfully contributed to the understanding of the kinetic processes related to water oxidation, particularly for TiO_2[15-16] and Fe_2O_3[17-22] photoanodes. However, there are relatively few TA studies of photocathodes for solar fuels production and to the best of our knowledge; this work represents the first TA study of a ZnTe photoelectrode for fuels production. Ultrafast TA spectroscopy has been reported for "magic-sized nanoclusters" and ZnTe quantum dot structures[14, 23-27] providing important insights into ultrafast exciton recombination, trapping, charge injection and charge separation on the fs-ns timescales. However, the physical properties and charge carrier dynamics of quantum confined ZnTe particles are likely to be markedly different to those of ZnTe photoelectrodes which often are formed of materials with far larger particle sizes (typically > 50 nm).[23, 28-30] Additionally, charge transfer during the surface catalysis steps of light-driven CO_2 reduction and proton reduction on semiconductor materials has been shown to often occur on the microseconds to milliseconds timescales.[16-17, 31-32] Therefore, a detailed TA spectroscopic investigation of ZnTe photocathodes within a photoelectrochemical cell across a wide range of time-scales, including those

relevant to both the fuel generation reactions and recombination loss pathways, is necessary to better understand the factors limiting the underlying efficiency of ZnTe phototocathodes.

In this work, thin, compact ZnTe films were synthesized by a thermal evaporation deposition method. Charge trapping and recombination in ZnTe films under potentionstatic control was monitored across a very wide range of timescales (ps-ms) using TA spectroscopy in the visible spectral region (450 – 950 nm) leading to the observation of a significant loss mechanism, the deep trapping of photogenerated electrons within ZnTe. Spectral features assigned to shallow trapped/conduction band electrons are also observed in the nIR (> 1150 nm) with these features being sensitive to the presence of an electron acceptor indicating that they are likely to be active towards CO_2 or H^+ at the electrode surface.

2. EXPERIMENTAL SECTION

2.1. Materials. ZnTe (99.99% metals basis) were purchased from Alfa Aesar. CH_3CN in spectrophotometric grade and other chemical reagents in analytical grade including $NaClO_4$, $AgNO_3$, Methyl viologen (MV) dichloride hydrate, 1,4-benzoquinone, Na_2SO_3 and tetra-n-butylammonium hexafluorophosphate were purchased from Sigma Aldrich. CO_2 and argon (CP grade) were purchased from BOC. Milli-Q ultrapure water was used throughout this study.

2.2. Synthesis of ZnTe. ZnTe films were grown on FTO substrates by thermal evaporating using a ZnTe target kept at room temperature. A tantalum boat was used as the source holder and the pressure inside the chamber is evacuated down to 4.5×10^{-5} Pa. The ZnTe films were evaporated thermally with a deposition rate of 0.2 nm/s with different thicknesses. The deposition rate and thickness were monitored during deposition using a quartz crystal monitoring system.

2.3. Characterization. X-Ray Diffraction measurement was carried out using a Panalytical X'Pert PRO HTS diffractometer. UV/Vis absorption spectroscopy was performed using a Shimadzu 2600

spectrometer. FT-IR spectra were recorded with a Bruker Vertex 70V Fourier-transform infrared spectrometer using a Near-IR globar source. The surface morphology of ZnTe was obtained by a Philips XL-30 field emission scanning electron microscope. The compositions of the ZnTe films are determined using a PSP Vacuum Technology X-ray source operating with an Al Kα X-rays at 144 W and a PSP Vacuum Technology Electron Energy Analyzer CHA.

2.4. Electrochemical measurement. The PEC performance of ZnTe was measured using a PalmSens^3 potentiostat under front-side illumination from a 300 W Xe lamp equipped with KG1 and 420 nm long pass filters. A custom designed photoelectrochemical cell with a ZnTe photocathode, a platinum sheet counter electrode and a 3.5 M NaCl Ag/AgCl reference electrode protected by a NaCl double junction was used in all experiments. The electrolyte used throughout was 0.1 M $NaClO_4$ and prior to all experiments it was thoroughly degassed with a stream of CO_2 or Ar for at least 30 minutes. Linear sweep voltammograms were recorded with chopped light at a scan rate of 10 mV s^{-1}.

2.5. Spectroelectrochemical measurements. Spectroelectrochemical measurements were performed in a sealed quartz cuvette (1 × 2 cm) with a Shimadzu 2600 spectrophotometer (500 – 900 nm) measuring in absorption mode or Bruker Vertex spectrometer (IR region) operating in transmittance mode. PalmSens^3 was used to control potential in all measurements, with the ZnTe film as working electrode, Pt sheet as the counter electrode and Ag/AgCl (3.5 M NaCl) as the reference electrode. The electrolyte used for Shimadzu 2600 spectrophotometer is 0.1 M $(But)_4NPF_6$/MeCN purged with Argon. The electrolyte used for FT-IR measurements is Argon-purged 0.1 M $NaClO_4$ aqueous solution. The infra spectra were recorded using air as the background, for 512 scans, at a resolution of 8 cm^{-1}.

2.6. Femtosecond and Microsecond Transient Absorption measurements. The Femtosecond and Microsecond TA spectroscopy apparatus has been described elsewhere.[18, 33] Briefly; Femtosecond TA spectroscopy was carried out using a PHAROS laser (Light Conversion, Ltd.) operating at 10 kHz

coupled to an ORPHEUS optical parametric amplifier (Light Conversion, Ltd.) in tandem with a LYRA harmonic generator (Light Conversion, Ltd.) to produce the desired wavelength for sample excitation. The pump beam intensity was adjusted with a neutral density filter so as to achieve approximately equal photon fluxes at different wavelengths. High electron-hole recombination rates are often observed with the high pump laser intensities and thus we use the relatively low pump intensity of ca. 50 μW and 400 μJ cm^{-2} for the femtosecond and microsecond TA experiment, in order to make the mechanistic data as comparable to solar irradiation as possible. However we do recognize the limitations of using short-pulsed laser excitation, hence we do not attempt to quantify recombination yields and quantitatively relate them to the photoelectrochemical data. The pump wavelength was tuned to 450 nm. A portion of the PHAROS output was also split off to pump a sapphire crystal to generate a white light continuum for the probe beam, which provided for spectral observation in the region 500−900 nm. The probe beam was focused to a spot size of ∼100 μm diameter on the sample and was overlapped completely by the pump beam. Spectra were acquired with a HELIOS transient absorption spectrometer (Ultrafast Systems, LLC). The time resolution of the setup is ∼400 fs. Measurements were performed by randomly stepping the optical delay line and averaging for 1 s at each delay time. Spectra of thin film samples were recorded in a quartz cuvette in CO_2-purged 0.1 M $NaClO_4$ solutions. Data were chirp corrected using the Surface Xplorer software package.

The microsecond TAS use the third harmonic of a Nd:YAG laser (Continuum, Surelite I-10, 355 nm, 4-6 ns pulse width) operating at 0.5 Hz. The repetition rate of the laser was chosen to ensure that all photogenerated charge carriers had fully decayed prior to the next excitation event. 355 nm laser was incident on the photoelectrochemical cell. A 75 W Xe lamp (OBB Corp.) coupled to monochromator (OBB Corp., set to 4 nm resolution) acts as the probe light and the change in optical density of the sample is calculated by measuring the transmitted light using a Si Photodiode (Hamamatsu) and a

homemade amplification system coupled to both an oscilloscope (Textronix TDS 220) and data acquisition card (National Instruments NI-6221). In order to generate the TA spectra at a range of biases, 300 laser shots per wavelength were recorded. The TA experiments were carried out in PEC cell in CO_2 or Ar purged 0.1 M $NaClO_4$ solutions under potentiostatic control at the potential indicated in the text, with the ZnTe films excited from the substrate-electrode side. Transient photocurrent measurements were recorded with the laser shot at the electrolyte-electrode side and the light from the Xe probe lamp was blocked. The current was obtained by measuring the voltage drop across a 47 ohm resistor in series with the working and counter electrode.

3. RESULTS

In this study, ZnTe films were synthesized using a thermal evaporation method described in the literature.[34-35] The characterization of the prepared ZnTe films can be found in the Supporting Information. Briefly, the XRD peaks ascribed to cubic ZnTe (JCPDS no. 01-001-0582) were identified, see Figure S1. But in the XPS spectrum, both Te^{2-} and Te^{4+} were observed. The appearance of Te^{4+} is commonly observed for ZnTe films due to the oxidation of Te^{2-} by the air and the formation of a surface layer of TeO_2 (Figure S2).[5] The brownish-red ZnTe films exhibited a broad absorption in the visible region with several weak absorption bands at ~530, ~625 and 730 nm and a tail extending to ~800 nm (Figure S3), following with onset of the band edge absorption at approximately 560 nm confirming the bandgap to be approximately 2.2 eV. The optical absorption at ~530 nm (2.34 eV) corresponds to the direct transitions along Γ direction from the valence band to conduction band,[36-38] and the absorption peaks at ~630 and 750 nm, with the transition energy lower than the bandgap value of ZnTe, possibly involved with the electronic transition in the mid-bandgap states. The SEM pattern of thin ZnTe films shows

that the films are uniform and have an average grain size of 120 ± 50 nm (Figure S4). The photoelectrochemical performance of ZnTe was monitored by linear sweep voltammetry under chopped visible light (50 mW cm^{-2}, 420 nm to 900 nm), measured in Ar and CO_2 saturated 0.1 M $NaClO_4$ solution using a three-electrode configuration, Figure 1. Under both Ar and CO_2 the ZnTe photocathode exhibited a cathodic photocurrent starting at approximately -0.45 V (*vs.* Ag/AgCl) and increasing as the bias was cathodically-shifted. Although the photocurrent response is similar under both gases it is notable that the magnitude of the photocurrent between -0.45 and -0.80 V was greater under CO_2. This is in line with past reports that CO_2 reduction was likely favored over proton reduction, demonstrating that these films are suitable models for our CO_2 reduction study by using TA spectroscopy.[8]

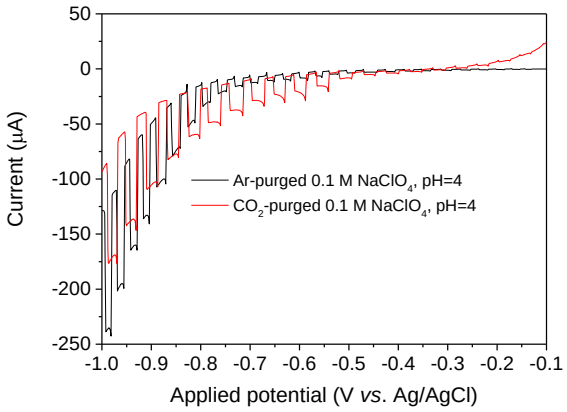

Figure 1. Linear Sweep Voltammogram shows the photocurrent-potential characteristics with the ZnTe photocathode in Ar and CO_2-saturated 0.1 M $NaClO_4$ aqueous solution (pH 4.0), under chopped visible light irradiation (50 mW cm^{-2}, 420 nm to 900 nm).

Ultrafast TA spectroscopy was initially used to probe the charge carrier dynamics of a ZnTe film at open circuit following 450 nm excitation in CO_2-purged 0.1 M $NaClO_4$ aqueous solution, Figure 2. Experiments under argon showed no significant differences to those recorded under

CO_2 therefore for clarity all transient spectroscopic data is presented under a single set of conditions (CO_2) in the main text. Equivalent experiments recorded under Ar are shown in the supporting information (Figure S5 and Figure S6). At very early timescales (2 ps) the spectra exhibit three broad absorbance bands at *ca*. 570, 630 and 850 nm due to initially photogenerated charge carriers (photogenerated electrons and/or holes), Figure 2A. Within *ca.* 40 ps of excitation the features at 630 and 850 nm become less pronounced and the adsorption peak at 570 nm blue-shifts to *ca.* 540 nm as carrier relaxation and trapping occurs. The strong absorption from *ca.* 540 nm and the weaker broad absorption across the visible region (maximum *ca.* 700 nm) are still present at the longest times that can be studied in this experiment (3 ns). The TA kinetics at single wavelengths are shown in Figure 2B. Normalizing the signals obtained in Figure 2B shows that the decays are probe wavelength dependent (Figure S7). The probe wavelength dependence of the decay kinetics is proposed to be due to changes in trap occupancies at early timescales leading to a change in the spectrum in the vis-NIR.[39-40] In particular we note a blue shift and narrowing of a spectral feature at *ca*. 570 nm (2 ps) which is assigned to shallow trapped/conduction band electrons relaxing into deep lying localized states.[40] The decay profile at 540 nm is well fitted with a minimum of two exponentials functions (4.8 ± 0.3 ps and 1384 ± 280 ps, Figure S8) with a significant portion of the decay trace (*ca.* 50%) appearing constant (concentration independent of time) across the ps-ns timescale, suggesting that charge carrier recombination occurs at times far greater than that probed in Figure 2. Probe wavelengths above 600 nm are indistinguishable but show complex decay kinetics, with the decay trace recorded at 800 nm requiring a minimum of 3 exponential functions (2.6 ± 0.2, 24.5 ± 2.5 and 363 ± 32 ps, Figure S8). Significantly *ca.* 17% of the transient absorption intensity at 800 nm is also apparently constant across the ps timescales. The complex multi-exponential

behaviour may be attributed to the availability of multiple states and trap sites across a wide range of energies, leading to complex charge carrier relaxation.[39-41]

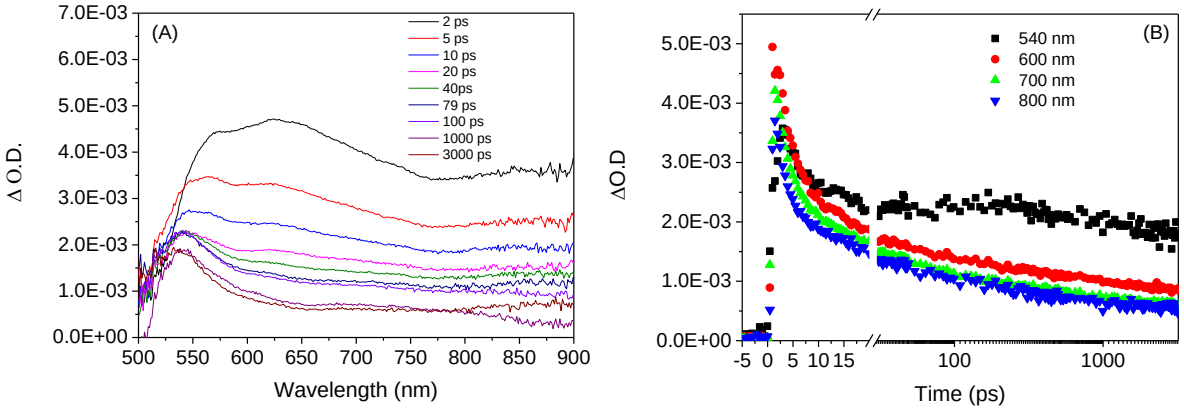

Figure 2. Transient absorption spectra (A) and decay dynamics at a single probe wavelength (B) of ZnTe, measured in CO_2-saturated 0.1 M $NaClO_4$ aqueous solution. The samples were excited by 450 nm laser with a power of 50 μW.

It is therefore apparent that a significant population of photogenerated charges have lifetimes well beyond the nanoseconds timescale. Recently slow TA experiments on the microseconds to seconds timescale have provided valuable insights into the dynamics of a range of processes including charge extraction via the external circuit, charge-carrier recombination and charge transfer reactions.[18-20] The slow TA spectrum of a ZnTe film, measured in the CO_2-purged 0.1 M $NaClO_4$ aqueous solution following excitation with 355 nm laser is shown in Figure 3. A broad positive absorption band peaking at 540 nm was observed in the visible to near-IR region (Figure 3A). It is clear that the shape of the TA spectra on slow timescales agrees well with that measured at the femtosecond spectra (Figure 2A), indicating the spectroscopic nature of the charge carriers does not change after 3 ns. Figure 3B shows two normalized decay traces obtained with the ZnTe probed at 540 and 750 nm. The decay traces yield a representative

lifetime ($t_{1/2}$) of 8 μs at open circuit and the charge carriers can persist to at least 10 ms, which is comparable to both TiO_2[15] and Fe_2O_3[22]. However, in contrast to the kinetic behavior observed on ultrafast timescales (Figure 2B), the decay trace at the microsecond to millisecond time range shows no probe wavelength dependence (Figure 3B). Similar overlap of the decay at 540 and 800 nm was also observed with the ZnTe films excited by 450 nm pump (Figure S9), indicating the probe-wavelength independent decays are not due to the difference in excitation condition. Furthermore, a dispersive power law decay dynamics ($\Delta O.D. \propto t^{-\alpha}$, $\alpha \approx 0.32$) is found in ZnTe on the microsecond timescale, see inset in Figure 3B. This is similar to the behavior of many semiconductor photoelectrodes where power law decay dynamics are indicative of non-geminate electron–hole recombination that proceeds via multiple trapping and de-trapping steps, characteristic of materials with a high density of trap states.[15, 17, 42] TA experiments have also been carried out with the ZnTe film held at a range of different applied potentials (Figure S10) to explore the bias dependent recombination. In past studies on solar fuels photoanodes charge carrier dynamics and recombination kinetics were strongly bias dependent,[15, 17] in contrast here we note only minimal differences in the kinetics probed at 540 and 750 nm with applied bias. A slight decrease in intensity of the photoinduced absorption feature at 540 nm is found at the most cathodic potentials but no significant change in lifetime is measured. Interestingly on both the ps-ns and μs-ms timescales the visible TA spectra were found to be remarkably insensitive to the choice of gas that the solution was purged with (CO_2 or Ar) or the presence of both electron donors (Na_2SO_3) and acceptors ($AgNO_3$, methylviologen, benzoquinone, O_2), see Figure S11 and Figure S12. However, the photocurrent of ZnTe film electrodes measured in the O_2-saturated solution is significantly larger than that measured in CO_2-saturated solution (Figure S13). These results indicate that the charge carriers observed by TA spectroscopy in the visible region are

either unable to reach the semiconductor/solution interface or that if present they lack the energetic driving force for charge transfer to the relevant acceptor/donor.

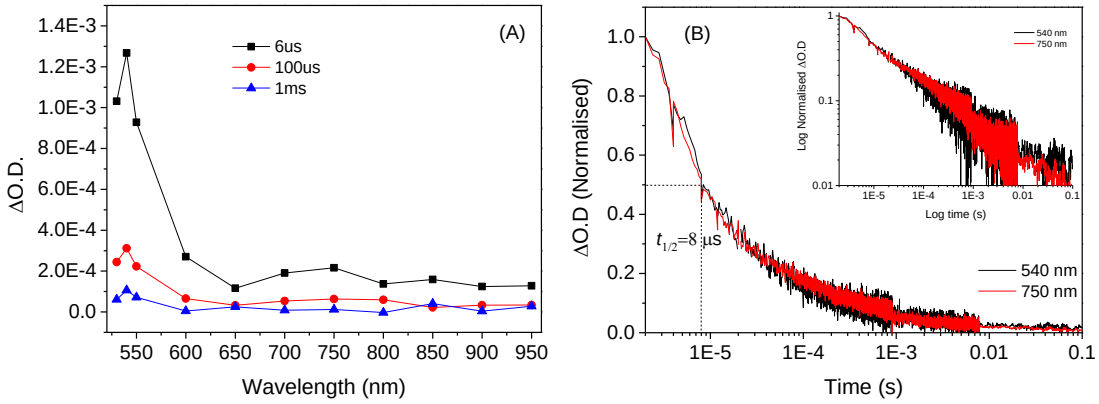

Figure 3. Transient absorption spectra (A) and normalized TAS decay traces recorded at 540 and 750 nm (B) of ZnTe, measured in CO_2-purged 0.1 M $NaClO_4$ aqueous solution. The samples were excited by 355 nm pump with an energy of 400 µJ cm^{-2}. The inset in Fig. 3B shows a log-log plot of the decay trace at 540 and 750 nm. The linear relationship indicated that a power law decay is occurring.

Transient Photocurrent (TPC) measurements of the ZnTe photocathode held at a range of different applied potentials are shown in Figure 4. The timescale during which current flow occurs gives a measure of the rate, and insights into the factors limiting, hole extraction to the external circuit. A fast initial decay of the transient photocurrent occurs during the first 10 µs of the measurement at all potentials studied and is not strongly dependent on the applied potential. This fast decay shows the similarity to the timescale of the TA decay at 540 nm and the minimal applied bias dependence may indicate that the two processes are associated, however it should be noted that the time resolution at the first 10 µs of these TPC measurements is limited by the instrument response and should be treated with caution. In contrast the TPC signal measured on the 20 µs - 0.1 s timescale is found to be dependent on the applied potential with the lifetime of

the TPC signal, and the associated total charge extracted, increasing as the bias was cathodically-shifted (Figure S14), with the trend well matching the photocurrent shown in Figure 1. The $t_{1/2}$ of the slower component of the TPC decay varied from *ca.* 30 µs to 180 µs between -0.25 and -0.8 V with significant current still present 1 ms after excitation at -0.8 V. The increased lifetime of the TPC coupled to an increase in the total level of charge extraction at more negative applied potentials may be indicative of a reduced rate of electron-hole recombination, a process that will be in kinetic competition with hole transport.

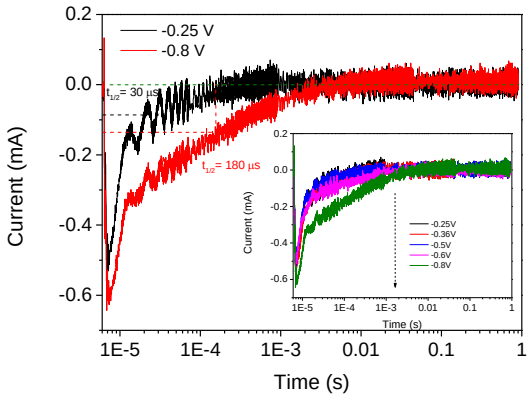

Figure 4. Transient photocurrent measurements measured on the TAS setup at -0.25 V and -0.8 V (*vs.* Ag/AgCl) for ZnTe film electrode respectively. The inset shows a series of transient photocurrents as a function of applied bias. The samples was illuminated by a laser (355 nm) from the Electrolyte-Electrode side with an average energy 400 µJ cm^{-2} and the CO_2-purged 0.1 M $NaClO_4$ aqueous solution was used as the supporting electrolyte.

To be able to rationalise the nature of the transient features at 540 and 700 nm observed on ZnTe photoelectrodes, spectroelectrochemical measurements in the dark have been carried out. To enable the build up of a population of charge carriers experiments were carried out in an aprotic solvent (Ar-purged 0.1 M $(But)_4NPF_6$/MeCN). The change in the UV/Vis absorption

spectrum at each potential is shown versus the spectrum at open circuit potential (*ca.* 0 V *vs.* Ag/Ag^+) in Figure 5. Even at potentials as positive as -0.1 V (*vs.* Ag/Ag^+) we begin to observe a strong absorption from *ca.* 500 to 600 nm with a maximum at approximately 550 nm in addition to a weaker absorptions at ~700 and 850 nm. These features are found to be insensitive to the presence of electron acceptor such as O_2 (Figure S15). The spectral features at 550 and 700 nm are in good agreement with those observed in TA experiments on the ps – ms timescales following initial carrier relaxation and on this basis we assign these TA features to photoelectrons localized in states close to the valence band edge. We rule out assignment of the positive absorption features to free electrons in the conduction band of ZnTe as the spectral features become apparent in the dark at potentials only 100 mV negative of the open circuit potential.

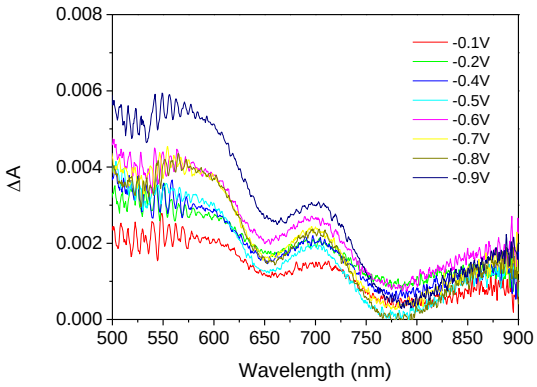

Figure. 5 Difference absorbance spectra of ZnTe electrode under argon in 0.1 M $(But)_4NPF_6$/MeCN, measured with the different applied potentials (*vs.* Ag^+/Ag). The values plotted in the Figure were obtained by subtracting the absorbance at 0 V (OCP) in every run.

It is well documented that the free conduction band electrons have a strong absorption in the IR region[28-29, 43] and numerous reports of shallow trapped photoelectrons in the nIR region exist.[44] Therefore in an attempt to identify the spectral signatures of photochemically active electrons in ZnTe we have also carried out a spectroelectrochemical study of ZnTe films in the nIR region (950 – 1450 nm). In the dark minimal changes were observed at wavelengths > 950 nm as the potential of the ZnTe film was changed from -0.27 to -0.90 V, Figure S16. However simultaneous illumination of the ZnTe film with UV light (390 nm) and application of a cathodic bias lead to large changes in the measured nIR spectrum, Figure 6. Between -0.24 to -0.90 V under illumination we observed the growth of a narrow absorption at 1153 nm and an increasing absorption at longer wavelengths from 1250 nm onwards (Figure 6A). The need for both UV illumination and a cathodic bias to generate these spectral features indicates that they can be assigned to accumulated photogenerated charges likely trapped in shallow states close to the conduction band edge (1153 nm) or within the conduction band itself (> 1250 nm). Unfortunately due to transient spectroscopy equipment limitations, it was not possible to probe at wavelengths greater than 950 nm, therefore to explore whether the photoelectrons detected in the nIR region are photochemically active experiments were carried out in the presence and absence of O_2. We have carried out photoelectrochemical studies with CO_2 and O_2 as electron acceptors and found that O_2 is a particularly effective electron scavenger on ZnTe making it easier to study the effect of adding an electron scavenger in our spectroscopic study, Figure S17. Significantly the light-induced absorption of ZnTe film electrodes measured at -0.7 V under illumination with the Ar-purged electrolyte was greatly reduced (> 50% at 1325 nm) when the film was exposed to the air (Figure 6B), demonstrating that the absorption features measured in

the near-IR region are related to a population of photogenerated charges that are able to undergo interfacial electron transfer.

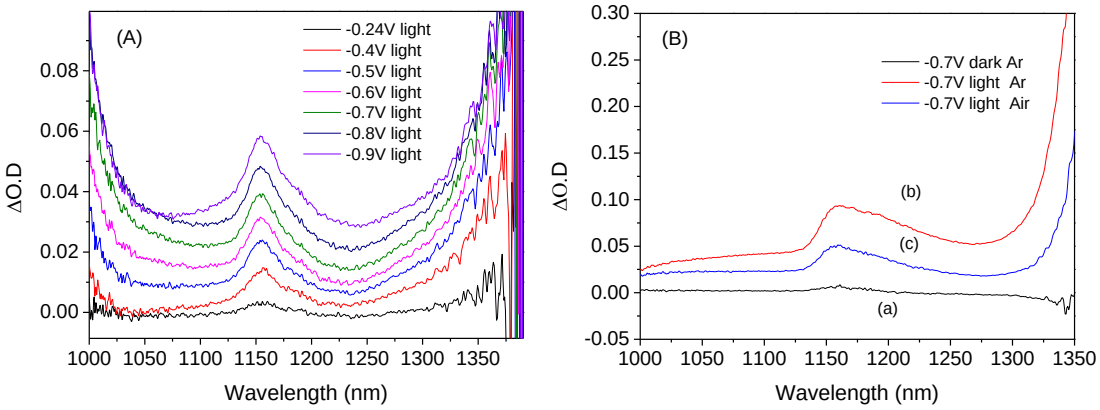

Figure 6. (A) Difference absorbance spectra of a ZnTe electrode under argon in 0.1 M $NaClO_4$, measured at different applied potentials (*vs*. Ag/AgCl) under LED (390 nm) illumination. (B) Difference absorbance spectra of another ZnTe electrode measured at -0.7 V with different condition: (a) in the dark with Ar-purged electrolyte, (b) LED irradiation with Ar-purged electrolyte and (c) LED irradiation with Air-purged electrolyte. The values plotted in the Figure were obtained by subtracting the absorbance at -0.24 V (OCP) in the dark.

4. DISCUSSION

A schematic summarising the key kinetic processes following photon absorption by a cathodically biased ZnTe electrode is shown in Figure 7. We propose charge trapping at a range of states with energies spanning from mid-gap to close to the valence band. Transient absorption spectroscopy using a UV/Vis probe provides limited information of the chemical nature of such trap sites, however past studies using chemically sensitive probes have also noted a range of states with those close to the VB being proposed to be related to the presence of Zn vacancies and/or impurity defects,[45-47] whilst mid-gap states related to isolated oxygen present on the metalloid sub-lattice and also Zn vacancies are also

reported.[48-50] On the basis of our spectroelectrochemcial studies we are able to assign the dominant spectral feature observed in the visible region during TA studies of a ZnTe photoelectrode to deeply trapped photoelectrons. Following the relaxation of electrons in these trap or mid-bandgap states (*ca*. 40 ps),[40] we find that these trapped electrons are largely insensitive to the presence of surface species indicating that the trap states are either located within the bulk of the semiconductor or they lack the thermodynamic driving force for electron transfer. Analysis of the slow decay kinetics of the deeply trapped electrons indicates that the charge-carrier recombination via a trapping-detrapping mechanism is the dominant decay pathway with charge carrier recombination occurring on the μs-ms timescale. TPC experiments appear to show two kinetic components with a faster portion with a lifetime similar to that of the deeply trapped electrons which indicate that deep-trap mediated recombination is in kinetic competition with hole transport to the external circuit, limiting the device efficiency.[18-20] Notably a bias dependent study of the decay kinetics of the deeply trapped electrons suggests that application of a cathodic bias leads to a only slight decrease in the yield of deeply trapped electrons on the μs-ms timescale, as seen through a decrease in the intensity of the 540 nm TA absorption, but no significant change in the slow kinetics of this feature (Figure S10). This minimal bias dependence of the kinetics of the 540 nm TA decay indicates that these electrons traps may exist deep within the electrode, outside of the space charge layer.

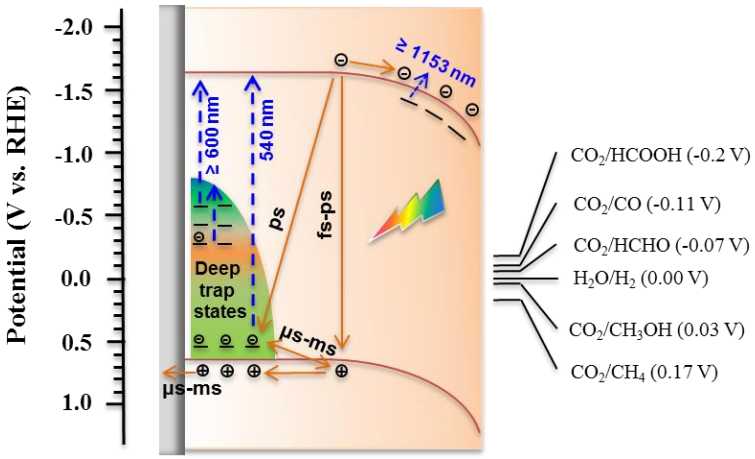

Figure 7. Schematic illustration of the relaxation processes involving photogenerated charge carriers in a p-type ZnTe film electrode under illumination. In the scheme, the solid line arrows represent the recombination, trapping and separation processes of charge carriers. The dashed line arrows represent transitions of trapped electrons.

Significantly a portion of the TPC is shown to be bias dependent with an increased lifetime for hole transport to the external circuit and a higher level of charge extraction at increasingly negative potentials. The TPC results are in line with expectations for a compact p-type photoelectrode which will display increased band bending and have a wider space charge layer under a cathodic bias, facilitating the rapid transport of photogenerated electrons to the electrode/electrolyte interface minimizing recombination losses with holes as they transport through the material.[1, 51] The presence of the slow bias dependent TPC signal that has kinetics that do not match those measured by TA spectroscopy indicates that a 2nd population of photoelectrons exist with absorption features outside the spectral range (UV-Vis) of our current TA apparatus.

Steady state experiments probing the nIR region in the presence and absence of O_2, a known electron acceptor, clearly demonstrate the presence of this hypothesised population of photoelectrons (Figure 6B). These shallow trapped charges are able to access the electrode/electrolyte interface and that they are chemically active, allowing us to suggest that the population of photoelectrons with spectral features in the nIR are those involved in CO_2 and H^+ reduction. Our steady state nIR spectroelectrochemical study also shows that the population of shallow trapped/conduction band charges increases with applied cathodic potential (Figure 6A), approximately following the change in photocurrent density (Figure 1). It is therefore apparent that as the degree of band-bending is increased charge transport to the surface is becoming competitive with bulk recombination and trapping of photoelectrons in deep lying states, rationalising the observed photocurrent plot, Figure 1. Notably state-of-the-art ZnTe/Au photoelectrodes[5-6] have been proposed to have enhanced activity due to the formation of a Schottky junctions that facilitates electron transport and accumulation at the ZnTe surface. This further highlights the importance of synthetic routes which improve the efficiency of electron accumulation at the ZnTe/electrolyte interface.

5. CONCLUSIONS

In this work, we have employed TA spectroscopy to monitor the charge carrier dynamics of ZnTe photocathodes across a range of timescales from picoseconds to seconds. A broad photoinduced absorption signal in the visible region with a maximum at 540 nm is formed within 40 ps of excitation and is assigned to deeply trapped electrons, likely in the bulk, that are inactive to surface species. The application of a cathodic bias and illumination is shown to lead to the formation of a 2nd spectral feature, monitored in the nIR by steady-state spectroelectrochemistry, due to the accumulation of photoelectrons

at near the surface. Our mechanistic studies provide a rationalisation for the observed photocurrent response with charge transport and accumulation at the surface becoming competitive with relaxation into deep lying inactive states at increasing cathodic potentials and reinforce the importance of developing synthetic modifications to improve band bending and facilitate charge separation.

Supporting Information Available.

Samples characterization data, transient absorbance spectroscopy in different environments, spectroelectrochemical measurements in the dark and photoelectrochemical measurements in the presence of CO_2 and O_2 can be found in the supporting information. This material is available free of charge via the Internet at http://pubs.acs.org.

ACKNOWLEDGEMENTS

We are grateful to Dr Max Birkett and Dr Tim Veal for assistance and access to the nIR measurements. We also acknowledge Mr Jonathan Lee and Dr Frank Jaeckel for assistance and access to the femtosecond TA spectrometer. Xianqiang thanks the funds from the China Scholarship Council for a Joint PhD. Student Program and the funds from the National Natural Science Foundation of China (No. 21377110) and Creative Research Group of NSFC (No. 21621005). AJC gratefully acknowledges a fellowship from the EPSRC (EP/ K006851/1). Unprocessed data is accessible free of charge at http://datacat.liverpool.ac.uk/.

REFERENCES

(1) Grätzel, M., Photoelectrochemical Cells. *Nature* **2001**, *414*, 338−344.

(2) Kumar, B.; Llorente, M.; Froehlich, J.; Dang, T.; Sathrum, A.; Kubiak, C. P., Photochemical and Photoelectrochemical Reduction of CO_2. *Annu. Rev. Phys. Chem.* **2012**, *63*, 541−569.

(3) Cowan, A. J.; Durrant, J. R., Long-Lived Charge Separated States in Nanostructured Semiconductor Photoelectrodes for the Production of Solar Fuels. *Chem. Soc. Rev.* **2013**, *42*, 2281−2293.

(4) Jang, J. W.; Cho, S.; Magesh, G.; Jang, Y. J.; Kim, J. Y.; Kim, W. Y.; Seo, J. K.; Kim, S.; Lee, K. H.; Lee, J. S., Aqueous-Solution Route to Zinc Telluride Films for Application to CO_2 Reduction. *Angew. Chemie Int. Ed.* **2014**, *126*, 5962−5967.

(5) Jang, Y. J.; Jang, J.-W.; Lee, J.; Kim, J. H.; Kumagai, H.; Lee, J.; Minegishi, T.; Kubota, J.; Domen, K.; Lee, J. S., Selective CO Production by Au Coupled ZnTe/ZnO in the Photoelectrochemical CO_2 Reduction System. *Energy Environ. Sci.* **2015**, *8*, 3597−3604.

(6) Jang, Y. J.; Jeong, I.; Lee, J.; Lee, J.; Ko, M. J.; Lee, J. S., Unbiased Sunlight-Driven Artificial Photosynthesis of Carbon Monoxide from CO_2 Using a ZnTe-Based Photocathode and a Perovskite Solar Cell in Tandem. *ACS nano* **2016**, *10*, 6980−6987.

(7) Jang, Y. J.; Lee, J.; Lee, J.; Lee, J. S., Solar Hydrogen Production from Zinc Telluride Photocathode Modified with Carbon and Molybdenum Sulfide. *ACS Appl. Mater. Interfaces* **2016**, *8*, 7748−7755.

(8) Chung, J.; Park, S. H.; Kim, E.-H.; Woo, S. I., Photoelectrochemical Production of Useful Fuels from Carbon Dioxide on a Polypyrrole-Coated p-ZnTe Photocathode under Visible Light Irradiation. *J. Mater. Chem. A* **2015**, *3*, 1089−1095.

(9) Sharma, I.; Singh, A. P.; Tyagi, N.; Saini, N.; Auluck, S.; Mehta, B. R., Oxygen Induced Enhanced Photoanodic Response of ZnTe:O Thin Films: Modifications in Optical and Electronic Properties. *J. Phys. Chem. C* **2017**, *121*, 1488−1497.

(10) Liu, X.; Li, D.; Yang, W.; Tang, S.; Li, X.; Fan, L.; Li, Y., Controlled Calcination of ZnSe and ZnTe Nanospheres to Prepare Visible-Light Catalysts with Enhanced Photostability and Photoactivity. *J. Mater. Sci.* **2016**, *51*, 11021−11037.

(11) Ehsan, M. F.; He, T., In Situ Synthesis of ZnO/ZnTe Common Cation Heterostructure and Its Visible-Light Photocatalytic Reduction of CO_2 into CH_4. *Appl. Catal. B Environ.* **2015**, *166*, 345−352.

(12) Ehsan, M. F.; Ashiq, M. N.; He, T., Hollow and Mesoporous ZnTe Microspheres: Synthesis and Visible-Light Photocatalytic Reduction of Carbon Dioxide into Methane. *RSC Adv.* **2015**, *5*, 6186-6194.

(13) Mahalingam, T.; John, V.; Rajendran, S.; Sebastian, P., Electrochemical Deposition of ZnTe Thin Films. *Semicond. Sci. Technol.* **2002**, *17*, 465−470.

(14) Kaniyankandy, S.; Rawalekar, S.; Verma, S.; Ghosh, H. N., Ultrafast Hole Transfer in CdSe/ZnTe Type II Core-Shell Nanostructure. *J. Phys. Chem. C* **2010**, *115*, 1428-1435.

(15) Cowan, A. J.; Tang, J.; Leng, W.; Durrant, J. R.; Klug, D. R., Water Splitting by Nanocrystalline TiO_2 in a Complete Photoelectrochemical Cell Exhibits Efficiencies Limited by Charge Recombination. *J. Phys. Chem. C* **2010**, *114*, 4208−4214.

(16) Cowan, A. J.; Leng, W.; Barnes, P. R.; Klug, D. R.; Durrant, J. R., Charge Carrier Separation in Nanostructured TiO_2 Photoelectrodes for Water Splitting. *PCCP* **2013**, *15*, 8772−8778.

(17) Barroso, M.; Pendlebury, S. R.; Cowan, A. J.; Durrant, J. R., Charge Carrier Trapping, Recombination and Transfer in Hematite (α-Fe_2O_3) Water Splitting Photoanodes. *Chem. Sci.* **2013**, *4*, 2724−2734.

(18) Forster, M.; Potter, R. J.; Ling, Y.; Yang, Y.; Klug, D. R.; Li, Y.; Cowan, A. J., Oxygen Deficient α-Fe_2O_3 Photoelectrodes: A Balance between Enhanced Electrical Properties and Trap-Mediated Losses. *Chem. Sci.* **2015**, *6*, 4009–4016.

(19) Le Formal, F.; Pendlebury, S. R.; Cornuz, M.; Tilley, S. D.; Grätzel, M.; Durrant, J. R., Back Electron-Hole Recombination in Hematite Photoanodes for Water Splitting. *J. Am. Chem. Soc.* **2014**, *136*, 2564–2574.

(20) Yang, Y.; Forster, M.; Ling, Y.; Wang, G.; Zhai, T.; Tong, Y.; Cowan, A. J.; Li, Y., Acid Treatment Enables Suppression of Electron-Hole Recombination in Hematite for Photoelectrochemical Water Splitting. *Angew. Chem. Int. Ed.* **2016**, *55*, 3403–3407.

(21) Pendlebury, S. R.; Barroso, M.; Cowan, A. J.; Sivula, K.; Tang, J.; Grätzel, M.; Klug, D.; Durrant, J. R., Dynamics of Photogenerated Holes in Nanocrystalline α-Fe_2O_3 Electrodes for Water Oxidation Probed by Transient Absorption Spectroscopy. *Chem. Commun.* **2011**, *47*, 716–718.

(22) Barroso, M.; Mesa, C. A.; Pendlebury, S. R.; Cowan, A. J.; Hisatomi, T.; Sivula, K.; Grätzel, M.; Klug, D. R.; Durrant, J. R., Dynamics of Photogenerated Holes in Surface Modified α-Fe_2O_3 Photoanodes for Solar Water Splitting. *Proc. Natl. Acad. Sci.* **2012**, *109*, 15640–15645.

(23) Zhang, J.; Rowland, C.; Liu, Y.; Xiong, H.; Kwon, S.; Shevchenko, E.; Schaller, R. D.; Prakapenka, V. B.; Tkachev, S.; Rajh, T., Evolution of Self-Assembled ZnTe Magic-Sized Nanoclusters. *J. Am. Chem. Soc.* **2015**, *137*, 742–749.

(24) Jin, S.; Zhang, J.; Schaller, R. D.; Rajh, T.; Wiederrecht, G. P., Ultrafast Charge Separation from Highly Reductive ZnTe/CdSe Type II Quantum Dots. *J. Phys. Chem. Lett.* **2012**, *3*, 2052–2058.

(25) Zhang, J.; Jin, S.; Fry, H. C.; Peng, S.; Shevchenko, E.; Wiederrecht, G. P.; Rajh, T., Synthesis and Characterization of Wurtzite ZnTe Nanorods with Controllable Aspect Ratios. *J. Am. Chem. Soc.* **2011**, *133*, 15324–15327.

(26) Rawalekar, S.; Kaniyankandy, S.; Verma, S.; Ghosh, H. N., Effect of Surface States on Charge-Transfer Dynamics in Type II CdTe/ZnTe Core-Shell Quantum Dots: A Femtosecond Transient Absorption Study. *J. Phys. Chem. C* **2011**, *115*, 12335−12342.

(27) Cadirci, M.; Stubbs, S.; Fairclough, S.; Tyrrell, E.; Watt, A.; Smith, J.; Binks, D., Ultrafast Exciton Dynamics in Type II ZnTe-ZnSe Colloidal Quantum Dots. *PCCP* **2012**, *14*, 13638−13645.

(28) Yoshihara, T.; Katoh, R.; Furube, A.; Tamaki, Y.; Murai, M.; Hara, K.; Murata, S.; Arakawa, H.; Tachiya, M., Identification of Reactive Species in Photoexcited Nanocrystalline TiO_2 Films by Wide-Wavelength-Range (400 - 2500 nm) Transient Absorption Spectroscopy. *J. Phys. Chem. B* **2004**, *108*, 3817−3823.

(29) Yamakata, A.; Vequizo, J. J. M.; Kawaguchi, M., Behavior and Energy State of Photogenerated Charge Carriers in Single-Crystalline and Polycrystalline Powder $SrTiO_3$ Studied by Time-Resolved Absorption Spectroscopy in the Visible to Mid-Infrared Region. *J. Phys. Chem. C* **2015**, *119*, 1880−1885.

(30) Roberti, T. W.; Cherepy, N. J.; Zhang, J. Z., Nature of the Power-Dependent Ultrafast Relaxation Process of Photoexcited Charge Carriers in II-VI Semiconductor Quantum Dots: Effects of Particle Size, Surface, and Electronic Structure. *J. Chem. Phys.* **1998**, *108*, 2143−2151.

(31) Tang, J.; Durrant, J. R.; Klug, D. R., Mechanism of Photocatalytic Water Splitting in TiO_2. Reaction of Water with Photoholes, Importance of Charge Carrier Dynamics, and Evidence for Four-Hole Chemistry. *J. Am. Chem. Soc.* **2008**, *130*, 13885−13891.

(32) Pastor, E.; Pesci, F. M.; Reynal, A.; Handoko, A. D.; Guo, M.; An, X.; Cowan, A. J.; Klug, D. R.; Durrant, J. R.; Tang, J., Interfacial Charge Separation in Cu_2O/RuO_x as a Visible Light Driven CO_2 Reduction Catalyst. *PCCP* **2014**, *16*, 5922−5926.

(33) Zwijnenburg, M.; Walsh, J.; Lee, J.; Draper, E.; King, S.; Jäckel, F.; Martijn, A.; Adams, D.; Cowan, A., Controlling Visible Light-Driven Photoconductivity in Self-Assembled Perylene Bisimide Structures. *J. Phys. Chem. C* **2016**, *120*, 18479−18486.

(34) Ibrahim, A.; El-Sayed, N.; Kaid, M.; Ashour, A., Structural and Electrical Properties of Evaporated ZnTe Thin Films. *Vacuum* **2004**, *75*, 189−194.

(35) Zia, R.; Saleemi, F.; Riaz, M.; Nassem, S., Structural and Optoelectrical Properties of ZnTe Thin Films Prepared by E-Beam Evaporation. *J. Electron. Mater.* **2016**, *45*, 4762−4768.

(36) Zaari, H.; Boujnah, M.; El Hachimi, A.; Benyoussef, A.; El Kenz, A., Optical Properties of ZnTe Doped with Transition Metals (Ti, Cr and Mn). *Opt Quant Electron* **2014**, *46*, 75−86.

(37) Ahmed, F.; Naciri, A. E.; Grob, J.; Stchakovsky, M.; Johann, L., Dielectric Function of ZnTe Nanocrystals by Spectroscopic Ellipsometry. *Nanotechnology* **2009**, *20*, 305702.

(38) Sato, K.; Adachi, S., Optical Properties of ZnTe. *J. Appl. Phys.* **1993**, *73*, 926−931.

(39) Bauer, C.; Boschloo, G.; Mukhtar, E.; Hagfeldt, A., Ultrafast Relaxation Dynamics of Charge Carriers Relaxation in ZnO Nanocrystalline Thin Films. *Chem. Phys. Lett.* **2004**, *387*, 176−181.

(40) Cherepy, N. J.; Liston, D. B.; Lovejoy, J. A.; Deng, H.; Zhang, J. Z., Ultrafast Studies of Photoexcited Electron Dynamics in γ and α-Fe_2O_3 Semiconductor Nanoparticles. *J. Phys. Chem. B* **1998**, *102*, 770−776.

(41) Zhang, J. Z., Interfacial Charge Carrier Dynamics of Colloidal Semiconductor Nanoparticles. *J. Phys. Chem. B* **2000**, *104*, 7239−7253.

(42) Godin, R.; Wang, Y.; Zwijnenburg, M. A.; Tang, J.; Durrant, J. R., Time-Resolved Spectroscopic Investigation of Charge Trapping in Carbon Nitrides Photocatalysts for Hydrogen Generation. *J. Am. Chem. Soc.* **2017**, *139*, 5216−5224.

(43) Szczepankiewicz, S. H.; Moss, J. A.; Hoffmann, M. R., Slow Surface Charge Trapping Kinetics on Irradiated TiO_2. *J. Phys. Chem. B* **2002**, *106*, 2922–2927.

(44) Tamaki, Y.; Furube, A.; Murai, M.; Hara, K.; Katoh, R.; Tachiya, M., Dynamics of Efficient Electron-Hole Separation in TiO_2 Nanoparticles Revealed by Femtosecond Transient Absorption Spectroscopy under the Weak-Excitation Condition. *PCCP* **2007**, *9*, 1453–1460.

(45) Dean, P.; Venghaus, H.; Pfister, J.; Schaub, B.; Marine, J., The Nature of the Predominant Acceptors in High Quality Zinc Telluride. *J. Lumin.* **1978**, *16*, 363–394.

(46) Magnea, N.; Bensahel, D.; Pautrat, J.; Pfister, J., Optical Identification of Substitutional Acceptors in Refined ZnTe. *Phys. Status Solidi B* **1979**, *94*, 627–639.

(47) Carvalho, A.; Öberg, S.; Briddon, P., Intrinsic Defect Complexes in CdTe and ZnTe. *Thin Solid Films* **2011**, *519*, 7468–7471.

(48) Kvit, A.; Medvedev, S.; Klevkov, Y. V.; Zaitsev, V.; Onishchenko, E.; Klokov, A.; Bagaev, V.; Tsikunov, A.; Perestoronin, A.; Yakimov, M., Deep-Level Optical Spectroscopy of ZnTe. *Phys. Solid State* **1998**, *40*, 924–929.

(49) Verity, D.; Bryant, F.; Scott, C.; Shaw, D., Deep Level Transient Spectroscopy of Hole Traps in Zn-Annealed ZnTe. *Solid State Commun.* **1983**, *46*, 795–798.

(50) Norris, C., The Origin of the 1.59 eV Luminescence in ZnTe and the Nature of the Postrange Defects from Ion Implantation. *J. Appl. Phys.* **1982**, *53*, 5172–5176.

(51) Bott, A. W., Electrochemistry of Semiconductors. *Curr. Sep.* **1998**, *17*, 87–92.

TOC Graphic

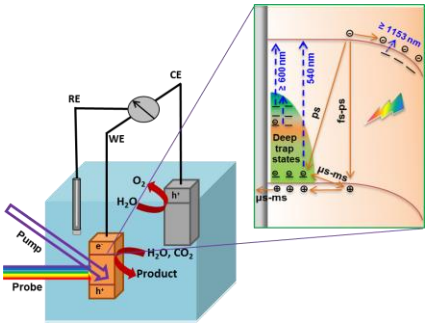
RE
CE
WE
O_2
H_2O
h⁺
e⁻
h⁺
Pump
Probe
H_2O, CO_2
Product
≥ 1153 nm
≥ 600 nm
540 nm
Deep trap states
ps
fs-ps
ns-ms
µs-ms